AIAA 94-1996

ELAFINT – A Mixed Eulerian–Lagrangian Method for Fluid Flows with Complex and Moving Boundaries

H. S. Udaykumar, W. Shyy and M.M.Rao
Department of Aerospace Engineering, Mechanics and Engineering Science
University of Florida
Gainesville, FL 32611

6th AIAA/ASME Joint Thermophysics and Heat Transfer Conference
June 20-23, 1994 / Colorado Springs, CO

ELAFINT: A Mixed Eulerian–Lagrangian Method for Fluid Flows with Complex and Moving Boundaries

H. S. Udaykumar, W. Shyy and M.M. Rao
Department of Aerospace Engineering, Mechanics and Engineering Science
University of Florida, Gainesville, FL 32611

Abstract

In this work a mixed Eulerian–Lagrangian technique is devised, hereinafter abbreviated as *ELAFINT* (Eulerian Lagrangian Algorithm For INterface Tracking). The method is capable of handling fluid flows in the presence of both irregularly shaped solid boundaries and moving/free phase boundaries. The position and shape of the boundary are tracked explicitly by the Lagrangian translation of marker particles. The field equations are solved on an underlying fixed grid as in Eulerian methods. The interface passes through the grid layout and details regarding the treatment of the cut cells so formed are provided. The issues involved in treating the internal boundaries are dealt with, with particular attention toward conservation and consistency in the vicinity of the interface. The method is tested by comparing with solutions from well–tested body–fitted coordinate methods. Test cases pertaining to forced and natural convection in irregular geometries and moving phase boundaries with melt convection are presented. The capability developed here can be beneficial in solving difficult flow problems involving moving and geometrically complex boundaries.

1. Introduction

Many fluid dynamics problems of practical interest involve irregularly–shaped boundaries. In some cases the boundaries also move and change shape [1,2]. Considerable efforts have been directed in the past toward simulating fluid flows in the presence of such boundaries which often separate distinct phases. For example, algorithms based on body–fitted coordinates have been extensively developed in the last two decades [3]. When the interface is not highly deformed, a single boundary–conforming grid arrangement is convenient for obtaining solutions to the transport equations [4,5]. However, the efficacy of the boundary–fitted grid deteriorates when the interface becomes highly distorted due to difficulty in obtaining smooth grid distributions. The situation can be further complicated when there are moving boundaries. The method experiences serious difficulties when interfaces merge or fragment. For highly deformed interface shapes purely Eulerian methods [2, 6–10] have been found to be useful, since in such methods the grid is completely independent of the interface and is usually of fixed Cartesian form. However, when details of the interface shape are to be explicitly tracked, the Eulerian methods are not suitable since in such methods the interface is deduced based on a computed fluid fraction field. In tracking highly distorted interfaces a combination of the strengths of Eulerian and Lagrangian methods will be desirable. Some efforts have been devoted recently to developing such methods [11–17]. Such methods, employing fixed structured grids afford simplicity and availability of well–tested, economical field solvers. The only moving component is the interface. The presence of the internal boundary that passes through the fixed grid layout calls for special treatment, since some of the control volumes in the domain are fragmented by the interface. Udaykumar and Shyy [11] have described some procedures designed to deal with the pure conduction system including the cut–cells. Quirk [14], has detailed some of the procedures involved in dealing with cell fragments in the framework of compressible, inviscid flows around stationary obstacles. However, the calculation of fluxes is not clear from that source. In Zeeuw and Powell [15] and Bayyuk et al. [16], a Cartesian grid is employed to track the motion of solid objects through an inviscid compressible fluid. Miyata [12] has employed a fixed grid formulation for the simulation of wave breaking. The treat–

ment of the free/moving surface in that work is not crucial to the physical phenomena under study and hence the treatment there is not very detailed. The physical problems discussed here are strongly affected by viscous effects and thus diffusion terms are to be included. Thus the full Navier–Stokes equations for incompressible flow including phase change are solved, with particular focus on the conservation of fluxes at the interface.

The system chosen for investigation is the solidification phenomenon, where the interface is in motion and there is transport of momentum and energy across the interface. In various solidification processing arrangements, conditions are encountered under which the interface separating the solid and liquid phases needs to be accurately resolved in order to simulate the transport and phase change processes [1, 18,19]. At the microscopic level, solid–melt interfaces experience morphological instabilities and break up into convoluted structures such as dendrites and cells [18]. At the macroscopic level, convective transport also causes the interface to display highly complicated characteristics in time and space [20,21]. In this work, we develop a numerical simulation technique called ELAFINT (for Eulerian Lagrangian Algorithm For INterface Tracking). The technique can handle the conditions that are encountered during a typical solidification process, viz.

a. the solid–liquid interface is a phase discontinuity, boundary conditions in each phase have to be applied for the fluid flow equations on this moving internal boundary. The interface is a source of heat, mass and momentum and can be arbitrarily distorted.

b. The method developed should be able to handle the solidification processes at the macro– and micro–scales.

c. Other demands on the solution procedure are similar to those on the pure conduction system [11].

The numerical simulation of solidification phenomena requires the solution of the transport equations in each phase. In the liquid phase the Navier–Stokes equations are solved subject to the Boussinesq approximation as given below.

Continuity :
$$\nabla \cdot \vec{u} = 0 \tag{1}$$

Momentum :
$$\frac{\partial \vec{u}}{\partial t} + \vec{u} \cdot \nabla \vec{u} = \nu \nabla^2 \vec{u} - \frac{\nabla p}{\varrho_o} - \beta (T - T_o)\ g\ \vec{j} \tag{2}$$

Energy :
$$\frac{\partial T}{\partial t} + \vec{u} \cdot \nabla T = \alpha_l \nabla^2 T \tag{3}$$

If necessary the Boussinesq approximation can be removed and the full Navier–Stokes equations solved in the melt.

In the solid phase:
$$\vec{u} = 0 \tag{4}$$

and energy equation reads:
$$\frac{\partial T}{\partial t} = \alpha_s \nabla^2 T \tag{5}$$

In the above equations, $\vec{u}$ is the velocity vector, p, T and ϱ are respectively the pressure, temperature and density. α, ν and β are thermal diffusivity, kinematic viscosity and thermal expansion coefficient respectively. Subscript o implies a reference value and l, s represent liquid and solid phases.

The field equations are solved subject to the following boundary conditions on the moving interface [18]:
$$T_{interface} = T_m\ (1 - \frac{\gamma}{L} \varkappa) \quad (Gibbs - Thomson\ \ condition) \tag{6}$$
where T_m is the melting temperature, γ is the surface tension, L the latent heat of fusion and $\varkappa$ the local curvature of the interface.

The fluid flow velocity boundary conditions are :
$$\vec{u} \cdot \vec{t} = 0 \quad (no - slip) \tag{7}$$
$$\varrho_L \vec{u} \cdot \vec{n} = (\varrho_s - \varrho_L) V_N \quad (mass\ \ conservation) \tag{8}$$
where $\vec{t}, \vec{n}$ are the tangent and V_N normal respectively is the normal velocity of the interface, given by,
$$\varrho_s L V_N = (k_s \frac{\partial T_s}{\partial n} - k_l \frac{\partial T_l}{\partial n}) \quad (Stefan\ \ condition) \tag{9}$$

Appropriate Neumann and Dirichlet conditions are applied at the boundaries of the computational domain. Boundary conditions for the equations in *each phase* are applied on this boundary, which requires that the curvature and slopes of the interface be obtained accurately. Eq. (9) is a statement of heat conservation across the phase discontinuity and inaccuracies in computing heat fluxes can lead to erroneous values of interface velocities. An efficient field equation solver needs to be developed which incorporates the information regarding interface shape and location. The boundary conditions are to be applied at the *exact location of the interface*. Conventional Lagrangian approaches, employing moving, boundary conforming grids fail when the interface becomes highly contorted and suffers topological changes. The Eulerian methods, solve for fluid fraction variables on stationary grids, and reconstruct the interface based on the fluid fraction data in each cell, a process that involves several logical operations. In order for the interfaces obtained to be accurate highly refined grids may be required. The computational procedure developed seeks to surmount the difficulties associated with conventional approaches by combining features of both methods. With this in view, Udaykumar and Shyy [22] developed an interface tracking procedure that can handle highly distorted fronts and their interactions. In this work we develop a complete algorithm called *ELAFINT* (for Eulerian −Lagrangian Algorithm For INterface Tracking) capable of solving fluid flow problems bounded by complex configurations and moving boundaries, arising from the phenomena such as materials solidification.

To solve the field equations a *fixed, Cartesian grid* is used to perform the computations. The irregularly shaped interface is tracked over this grid and is represented using *marker particles*. The markers are connected by piecewise circular arcs to obtain interfacial shape information such as normals and curvatures. The interface is advanced in time by the Lagrangian translation of the marker particles, the normal velocity being computed from Eq. (9). The new interfacial shape is obtained by joining these updated markers. The use of an Eulerian grid facilitates the execution of merger/ breakup procedures at the interface, a drawback conventionally attached to pure Lagrangian methods. The Lagrangian component of the present method allows the interface to be accurately captured, which on the other hand, is a significant improvement over the conventional Eulerian methods. In conjunction with the interface tracking procedure, a pressure−based control volume formulation is designed to solve the field equations. Since the interface cuts through the grid, fragmented control volumes may arise in the cells containing the interface. The present algorithm uses integration formulas consistent with the underlying discretization scheme to handle such cases. The basic features of the methodology presented here were developed in the case of pure conduction in previous work by Udaykumar and Shyy [11]. The ability to handle highly distorted interface and to follow interfacial evolution accurately over long time durations was demonstrated in that work.

In the following, we describe for a general conserved variable ϕ, the application of a control volume formulation and the discretization scheme for a two−dimensional geometry. In Section 2 we clarify the treatment of the individual terms for each of the flow variables, explain the various issues involved, and address the conservation and consistency aspects in the computational notation of the pressure−based methodology. We then present some test cases and comparisons to validate the solution procedure.

2. The control volume formulation for a transport variable ϕ

2.1 Discretization

Consider the conservation law for the variable ϕ, defined to be (a) 1 for the continuity equation (b) u and v for the x and y momentum equations and (c) specific enthalpy for the energy equation. In the general case, we have

$$\frac{\partial(\rho\phi)}{\partial t} + \nabla \cdot (\rho\vec{u}\phi) = (\nabla \cdot \Gamma\nabla\phi) + S \qquad (10)$$

Consider the interface that passes through a Cartesian grid at a given instant. The control volumes in the vicinity of the interface are irregularly shaped, and in the most general case can assume a five−sided shape as shown in Figure 1 below.

In order to evaluate the momentum fluxes through the cell faces, we integrate Eq. (10) over the control volume and employ the divergence theorem to get

$$\int_V \frac{\partial \varrho\phi}{\partial t} dV + \int_A (\varrho\vec{u}\phi) \cdot \vec{n} dA = \int_A (\Gamma \nabla\phi) \cdot \vec{n} dA + \int_V S dV \qquad (11)$$

In two–dimensions we have

$$\int_A \frac{\partial \varrho\phi}{\partial t} dA + \oint_l (\varrho\vec{u}\phi) \cdot \vec{n} dl = \oint_l (\Gamma \nabla\phi) \cdot \vec{n} dl + \int_A S dA \qquad (12)$$

where the second term on the left hand side is now the line integral of the outward normal convective fluxes and the first term on the right side is the line integral of the outward normal diffusion fluxes through the faces of the control volume.

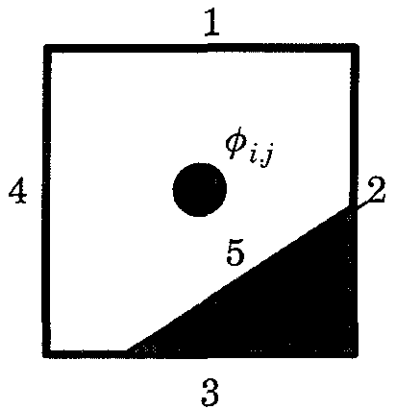

Figure 1

A typical control volume encountered in the mixed Eulerian–Lagrangian method.

We now proceed to discretize each of the terms in Eq. (12) for the control volume shown. Thus

$$\int_A \frac{\partial \varrho\phi}{\partial t} dA = \frac{\varrho^{n+1}{}_{ij}\phi^{n+1}{}_{ij} - \varrho^{n}{}_{ij}\phi^{n}{}_{ij}}{\delta t} A_{cv} \qquad (13)$$

where the superscript n, $n+1$ indicate the time levels and δt is the time step size. A_{cv} is the area of the irregular control volume. Next,

$$\oint_l (\varrho\vec{u}\phi) \cdot \vec{n} dl = \sum_{k=1}^{5} (\varrho_k u_k \phi_k)^{n+1} dl_k \qquad (14)$$

is the summation of the convective normal effluxes through each cell face of the control volume. The superscript $n+1$ indicates the implicit nature of the scheme. The diffusion fluxes are computed as

$$\oint_l (\Gamma \nabla\phi) \cdot \vec{n} dl = \sum_{k=1}^{5} (\Gamma_k (\frac{\partial \phi}{\partial n})_k)^{n+1} dl_k \qquad (15)$$

Let us denote the source term as follows,

$$\int_A S dA = \bar{S} \qquad (16)$$

Substituting the above Eqs. (13–16) in Eq. (12) one obtains the discretised form as

$$\frac{\varrho^{n+1}{}_{ij}\phi^{n+1}{}_{ij} - \varrho^{n}{}_{ij}\phi^{n}{}_{ij}}{\delta t}A_{cv} + \sum_{k=1}^{5}(\varrho_k u_k \phi_k)^{n+1}dl_k = \sum_{k=1}^{5}(\Gamma_k(\frac{\partial\phi}{\partial n})_k)^{n+1}dl_k + \bar{S} \tag{17}$$

In particular the discrete form of the continuity equation can be written as

$$\frac{(\varrho^{n+1}{}_{ij} - \varrho^{n}{}_{ij})}{\delta t}A_{cv} + \sum_{k=1}^{5}(\varrho u_n)_k dl_k = 0 \tag{18}$$

Now multiplying Eq. (18) by the value $\phi_{i,j}$ and subtracting from Eq. (17) gives

$$\frac{\varrho^{n}{}_{ij}(\phi^{n+1}{}_{ij} - \phi^{n}{}_{ij})}{\delta t}A_{cv} + \sum_{k=1}^{5}\varrho_k u_k(\phi_k - \phi^{n+1}{}_{ij})^{n+1}dl_k = \sum_{k=1}^{5}(\Gamma_k(\frac{\partial\phi}{\partial n})_k)^{n+1}dl_k + \bar{S} \tag{19}$$

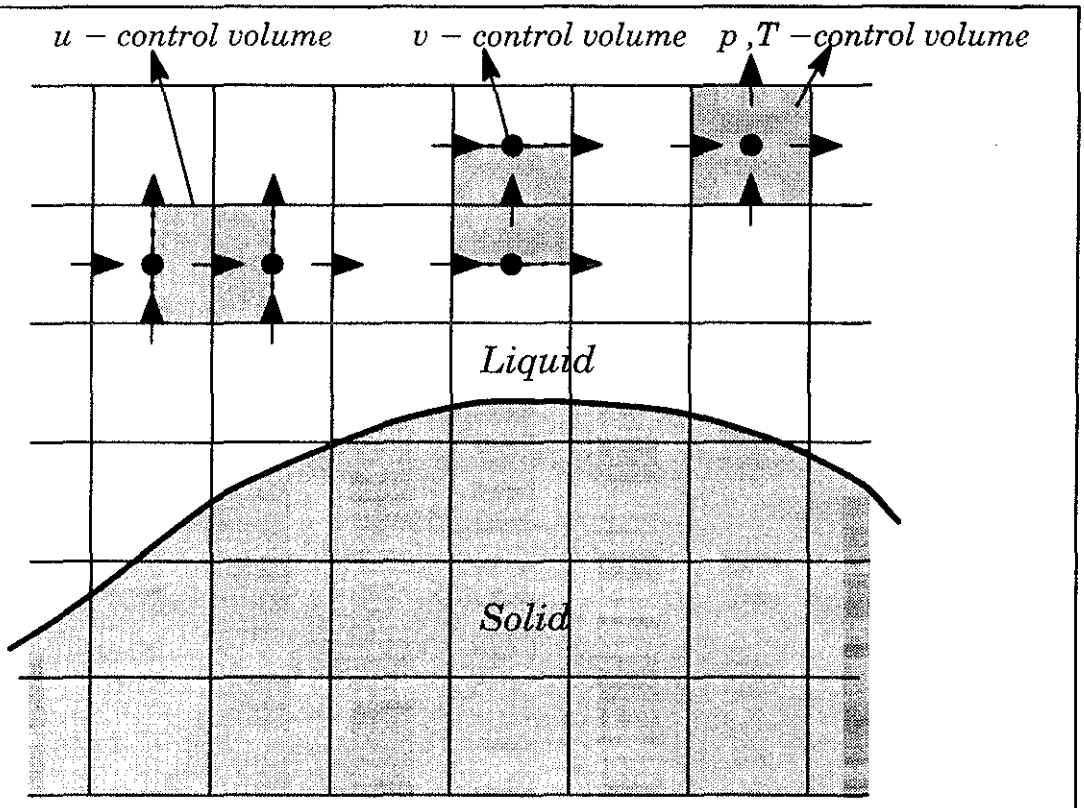

Figure 2

Control volumes for u, v , p and T variables showing the staggered arrangement.

2.2 The staggered grid

The solution of the discrete form, namely Eq. (19) is carried out on a staggered grid arrangement shown in Figure 2. Staggered grids have been extensively adopted for computation of incompressible fluid flows due to their many advantages [24, 25]. The variables and their respective control points are located as indicated in Figure 2. The interface is thus required to be tracked on such a grid arrangement. The definition of the control volumes, which is carried out according to the intersection procedure is now applicable

to each type of control volume shown, namely the u, v and (p,T) control volumes. For a given control volume then, the interface tracking procedure provides the information shown in Figure 3 .Thus, at each iteration, explicit definition of the interface location/control volumes for each variable and its grid is available. This facilitates the application of boundary conditions on the faces of the cells containing the interface, as explained later.

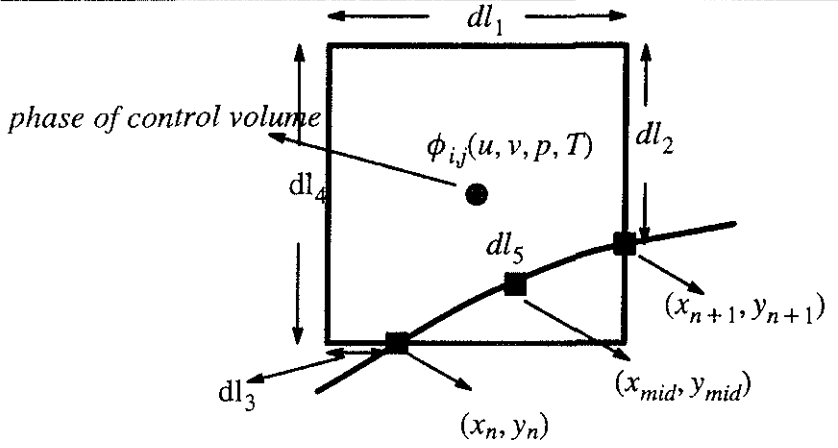

Figure 3
Illustration of information provided by the interface tracking module during assembly of coefficients for control volumes

2.3 Computation of the pressure field

For incompressible flows, since no explicit equation exists for the pressure field, some means needs to be devised to compute the pressure field. To extract the pressure, one makes use of the continuity equation and obtains a correction equation for the pressure and velocities that enforces mass conservation. The correction procedure is continued until until convergence is achieved for each time step. Such a pressure correction method has been widely used and is described in detail elsewhere [24,25]. The essential feature is that the following equation results for the pressure correction at each point

$$\begin{aligned} a_P p'_P - a_N p'_N - a_S p'_S - a_E p'_E - a_W p'_W &= \\ \frac{(\varrho_P^o - \varrho_P)A_{cv}}{\delta t} + \varrho_w u_w dl_w - \varrho_e u_e dl_e + \varrho_s v_s dl_s - \varrho_n v_n dl_n & \end{aligned} \qquad (20)$$

where the right hand side represents the mass deficit in the control cell, and is required to be nullified at convergence. The individual terms on the right hand side are mass fluxes through the faces of the control volume, including the interfacial segments.

2.4 Computation of convective and diffusive fluxes and source terms

Returning now to the Eq. (19) , for the situation shown in Figure 4 below. For the variable ϕ, the convective fluxes are evaluated as follows

$$\begin{aligned} \sum_{k=1}^{5}(\varrho u_n)_k(\phi_k - \phi_P)dl_k &= (\varrho_e u_e)(\phi_e - \phi_P)dl_e - (\varrho_w u_w)(\phi_w - \phi_P)dl_w \\ &+ (\varrho_n u_n)(\phi_n - \phi_P)dl_n - (\varrho_s u_s)(\phi_s - \phi_P)dl_s \pm (\varrho_I u_{nI})(\phi_I - \phi_P)dl_I \end{aligned} \qquad (21)$$

which may be written as,

$$\sum_{k=1}^{5}(\varrho u_n)_k(\phi_k - \phi_P)dl_k = F_e(\phi_e - \phi_P) - F_w(\phi_w - \phi_P) + F_n(\phi_n - \phi_P) - F_s(\phi_s - \phi_P) \pm \varrho_l u_{nl}(\phi_l - \phi_P)dl_l \quad (22)$$

Here the F's stand for the mass fluxes through the faces of the control volume. The lower case subscripts indicate the values at the cell faces. the manner in which these fluxes are evaluated , i.e., the specific shape function assumed for the variable ϕ for evaluation of these fluxes determines the order of accuracy of the scheme employed. In Eq. (22) the sign of the last term is to be decided. What is required is the outward normal flux from the interfacial segment. We shall return to this point momentarily.

Now, the diffusion fluxes can be written as

$$\sum_{k=1}^{5}\Gamma_k(\frac{\partial\phi}{\partial n})_k dl_k = \Gamma_e(\frac{\partial\phi}{\partial x})_e dl_e - \Gamma_w(\frac{\partial\phi}{\partial x})_w dl_w + \Gamma_n(\frac{\partial\phi}{\partial y})_n dl_n - \Gamma_s(\frac{\partial\phi}{\partial y})_s dl_s \pm \Gamma_l(\frac{\partial\phi}{\partial y})_l dl_l \quad (23)$$

Substituting the expressions provided by Eqs. (22) and (23) in Eq. (19) and simplifying, we now obtain

$$\frac{\varrho_P{}^o(\phi_P - \phi_P{}^o)A_{cv}}{\delta t} + (J_e - F_e\phi_P) - (J_w - F_w\phi_P) + (J_n - F_n\phi_P) - (J_s - F_s\phi_P) = \pm \Gamma_l(\frac{\partial\phi}{\partial n})_l dl_l \mp \varrho_l u_{nl} dl_l(\phi_l - \phi_P) + \bar{S} \quad (24)$$

where

$$J_e = \varrho_e u_e dl_e \phi_e - \Gamma_e(\frac{\partial\phi}{\partial x})_e dl_e \quad (25)$$

and

$$J_n = \varrho_n v_n dl_n \phi_n - \Gamma_n(\frac{\partial\phi}{\partial y})_n dl_n \quad (26)$$

with similar expressions for J_w and J_s. The following notation is standard for the SIMPLE algorithm [24]

$$J_e - F_e\phi_P = a_E(\phi_P - \phi_E) \quad (27)$$

$$J_w - F_w\phi_P = a_W(\phi_W - \phi_P) \quad (28)$$

with similar expressions for a_N and a_S. The forms assumed by $a_{E,W,N,S}$ determine the order of accuracy of the differencing scheme employed. For example,

$$a_E = D_e A(|P_e|) + [-F_e, 0] \quad (29)$$

where P_e is the cell Peclet number $= F_e/D_e$ and the square bracket implies the maximum of the two quantities. In this work the second–order central difference scheme is employed to discretize spatial derivatives, for which [24]

$$A(|P|) = 1 - 0.5|P| \quad (30)$$

The Eq. (24) can now be written as

$$\frac{\varrho_P{}^o(\phi_P - \phi_P{}^o)A_{cv}}{\delta t} + a_E(\phi_P - \phi_E) - a_W(\phi_W - \phi_P) + a_N(\phi_P - \phi_N) - a_S(\phi_S - \phi_P) = \pm \Gamma_l(\frac{\partial\phi}{\partial n})_l dl_l \mp \varrho_l u_{nl} dl_l(\phi_l - \phi_P) + \bar{S} \quad (31)$$

Letting

$$\frac{\varrho_P{}^o A_{cv}}{\delta t} = a_P{}^o \quad (32)$$

and

$$a_P = a_P{}^o + a_E + a_W + a_N + a_S \quad (33)$$

we have the final discretized form

$$a_P\phi_P = a_N\phi_N + a_S\phi_S + a_E\phi_E + a_W\phi_W + b \quad (34)$$

where

$$b = \overline{S} \pm \Gamma_I(\frac{\partial\phi}{\partial n_I})dl_I \mp \varrho_I u_{nI} dl_I(\phi_I - \phi_P) \quad (35)$$

In the above discretization, the value of ϕ at any point P is dependent on its four immediate neighbours. When cast in matrix form the equation reads–

$$[C]\ [\Phi] = [B] \quad (36)$$

where [C] is a pentadiagonal coefficient matrix, Φ is the solution vector and B is a source vector. The procedure usually adopted is to solve the system of equations in iterative fashion employing a line SOR method which calls for a tridiagonal matrix solution procedure.

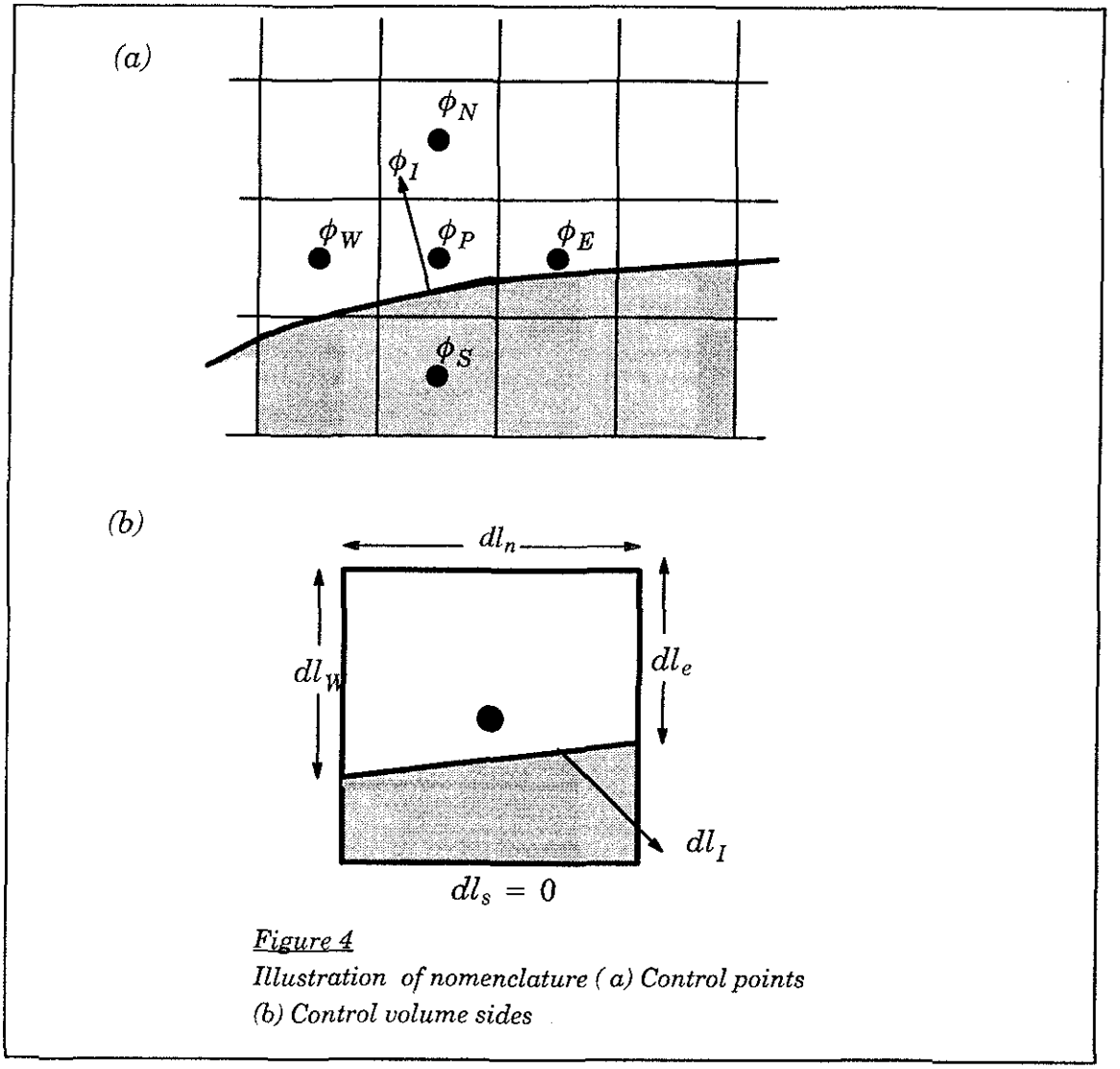

Figure 4
Illustration of nomenclature (a) Control points
(b) Control volume sides

2.5 Computation of interfacial fluxes

We now proceed to detail the method for obtaining the interfacial flux terms. Considering the fluxes from the interface,

$$\pm \Gamma_f(\frac{\partial \phi}{\partial n})_I \mp \varrho_I u_{nI} dl_I(\phi_I - \phi_P) \qquad (37)$$

We need to estimate the following quantities at the interface ;

$$(\frac{\partial \phi}{\partial n})_I \ , \ \varrho_I u_{nI} \ , \ \phi_I \qquad (38)$$

and determine the missing signs to evaluate the flux terms. As for the above values at the interface, ϱ_I is easily obtained for incompressible flow as the value of the density at the liquid control point closest to the interface. u_{nI} , the fluid velocity normal to the interface is evaluated from the boundary condition at the interface, Eq. (9), once the interfacial velocity at that point is known. The interfacial velocity is of course determined from the Stefan condition during the course of the calculation and is coupled to the temperature gradients in the vicinity of the interface. The normal gradient of any variable ϕ , i.e., $(\partial\phi/\partial n)_I$ is evaluated in the same fashion as for the pure conduction problem. A probe is inserted in each phase and a biquadratic shape function is described in the vicinity of the interface. The derivative can then be estimated. The value of the variable on the interface, ϕ_I is again obtained from the boundary conditions. In particular, for :

1. The u−momentum equation, $\phi = u$, and $u_I = u_{nI}\, n_x$ as shown in Fig. (5).
2. The v−momentum equation $\phi = v$, and $v_I = v_{nI}\, n_y$ as shown in Fig. (5).
3. For the energy equation, $\phi = T$ and T_I is obtained from the Gibbs−Thomson condition at the interface.

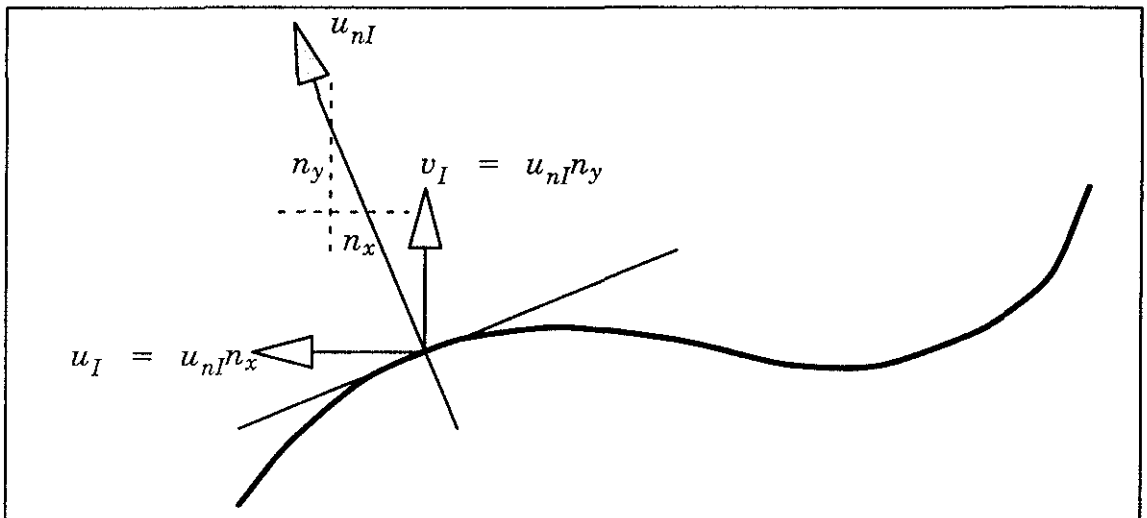

Figure 5

Illustration of velocity components of fluid at the interface

Next, we need to decide upon the signs to be assigned to each of the interfacial fluxes. The diffusion flux with the as yet undetermined sign is

$$\pm \Gamma_f(\frac{\partial \phi}{\partial n})_I dl_I \qquad (39)$$

The positive sign is applicable when an outflux is evaluated. By the procedure outlined above, the gradient evaluated is as follows :

$$\frac{\partial \phi}{\partial n} = (\frac{\phi_{I+dn} - \phi_I}{dn}) \qquad (40)$$

for the situation shown in Figure (6).

The gradient as evaluated above represents the influx into the control volume in each phase. A negative sign is therefore required to provide the efflux from the control volume. As for the sign of the convective interfacial flux, we have adopted the convention that the interface points into the liquid phase. Hence, u_{nI} is the normal velocity of the fluid at the interface, and is directed into the liquid control volume. Therefore, the convective flux into the control volume is given by

$$\varrho_I u_n dl_f(\phi_I - \phi_P) \qquad (41)$$

To obtain an efflux from the control volume, a negative sign should appear in front of this flux term. Thus, the final form of the source term b is given by,

$$b = -\Gamma_f dl_f(\frac{\partial \phi}{\partial n})_I + \varrho_I u_n dl_f(\phi_I - \phi_P) + \overline{S} \qquad (42)$$

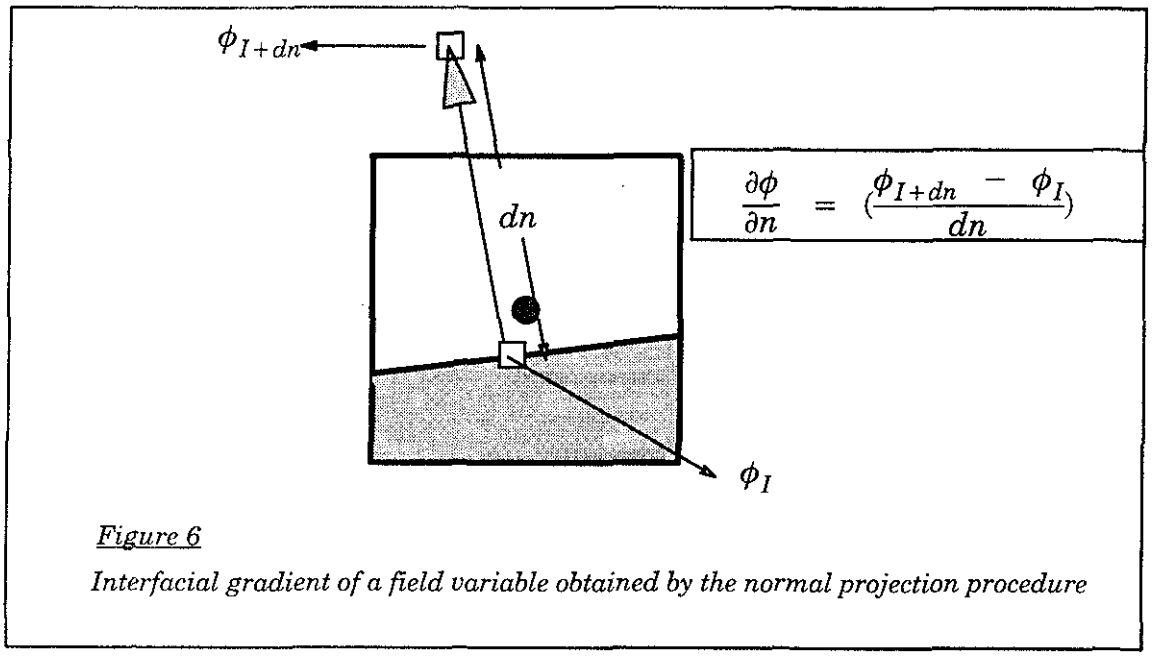

Figure 6

Interfacial gradient of a field variable obtained by the normal projection procedure

2.6 Evaluation of the source term

For each of the equations, namely the continuity and momentum equations, the source term $\overline{S}$ assumes a different form. The pressure terms are included in this source term and its evaluation involves certain considerations which we now detail. For the u−momentum equation for example, we have

$$\overline{S}_u = \int_A -(\frac{\partial p}{\partial x})\, dA \qquad (43)$$

and for the v−momentum equation

$$\overline{S}_v = \int_A -(\frac{\partial p}{\partial y})\, dA \qquad (44)$$

Consider the term corresponding to the u−momentum equation as in Eq. (43), in relation to the u−control volume shown in Figure 7(a) below. Applying the divergence theorem, Eq. (43) can be written as

$$\overline{S}_u = -\sum_{k=1}^{5} p_i(dl_y)_k \qquad (45)$$

where the length dl_y is the projected length of a side along the y−direction. Thus, for the control volume shown, the pressure contributions take the form,

$$\overline{S}_u = -p_e dl_e + p_w dl_w \pm p_f(dl_I)_y \qquad (46)$$

Now, as shown in Figure 7(b), $(dl_I)_y = dl_I\, n_x$, where n_x is the x−component of the unit normal vector to the interface in that cell, and is already available from the interface tracking information. From observing Figure 7(b) , it is evident that for $n_x < 0$ a negative sign is required in front of the pressure term for the interfacial segment and for $n_x > 0$, a positive sign is required. Thus, the appropriate form for the

source term is now

$$\bar{S}_u = -p_e dl_e + p_w dl_w + p_I dl_I n_x \qquad (47)$$

To estimate the value of pressure at the interface, p_I, a bilinear extrapolation is performed from the neighbouring liquid phase pressure control points onto the interface location.

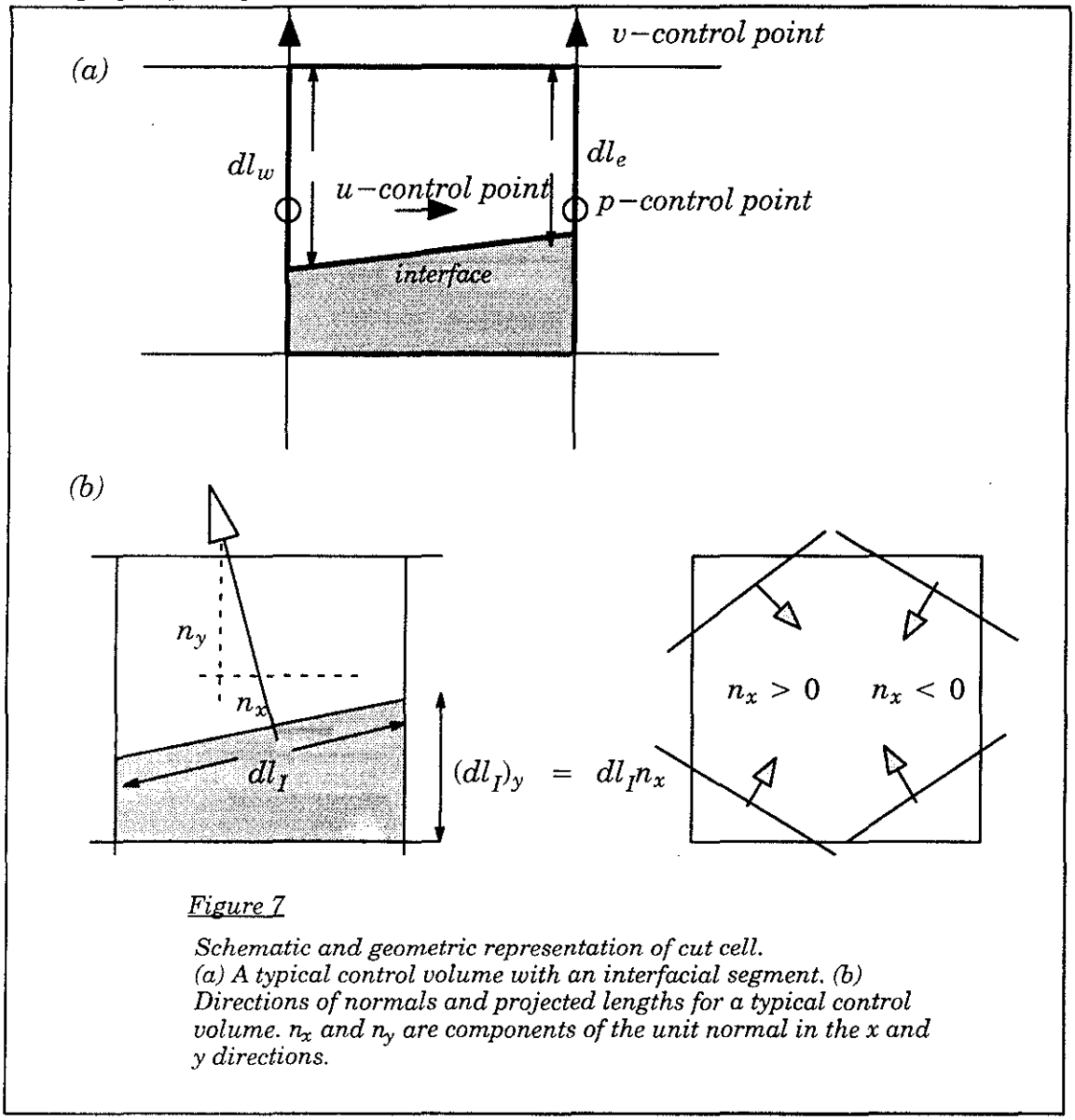

Figure 7

Schematic and geometric representation of cut cell. (a) A typical control volume with an interfacial segment. (b) Directions of normals and projected lengths for a typical control volume. n_x and n_y are components of the unit normal in the x and y directions.

2.7 The continuity equation : pressure correction equation

The pressure correction equation is of the form shown in Eq. (20). The right hand side contains mass fluxes through each side of the control volume. Such terms are easily evaluated, since the velocity values required in computing the mass fluxes are available at the cell faces, a feature of the staggered grid. The coefficients for the pressure correction equation are assembled in the standard way.

2.8 Dealing with cut cells

When the interface passes through the staggered grid arrangement as shown in Figure 2, the control volumes in the vicinity of the interface become fragmented. Consider the control volume for the u−velocity

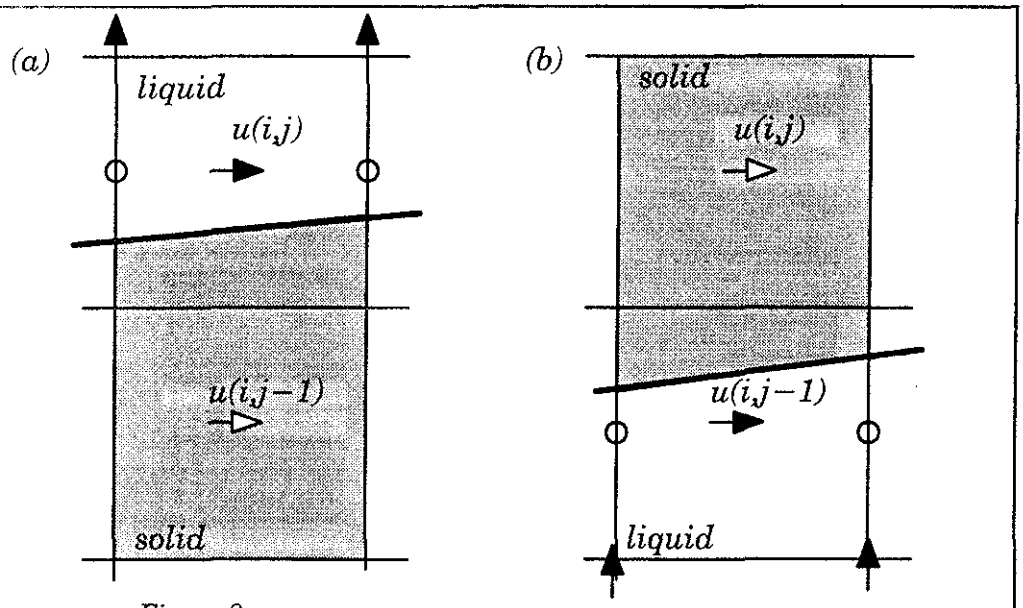

Figure 8
Definition of cut cells and their partners

u(i,j) as shown in Figure 8(a) below. The u control point lies in the liquid phase here while a piece of the control volume shown shaded lies in the solid phase. However, in Figure 8(b) the shaded region belongs to cell (i,j−1) but lies in the solid phase. Thus, one has to account for the existence of such fragments of control volumes and assign them to the proper phase. This is done by defining partner cells for each type of cell, a procedure discussed in more detail in [11]. In Figure 8(a) for example the cell (i,j) is now redefined to be the unshaded irregular cell. Similarly, in Figure 8(b) the new u−cell (i,j) is defined by the shaded region. This procedure of redefining the cut cells and their partners is accomplished by running through the array of interfacial cells. By assigning partner cell fluxes and redefining dimensions it is possible to maintain consistency at cell faces and conservation of fluxes.

2.9 Conservation and consistency at cell faces

In solving the set of conservation laws, it is important to set up the control volume formulation and differencing schemes so that strict conservation of fluxes is maintained. Consider the situation shown in Figure 9. Of concern to us are the flux evaluation through the faces of the cells (i,j) and (i ± 1, j) and their relation to the partner cell definitions. The newly redefined cells after partner cell assignment are as shown by the dotted line. The fluxes through the west face of (i,j) are now magnified by the factor (dl_w(i,j) + (dy−dl_w(i,j−1))) / dl_w(i,j) to correct for the augmented length of the west face. A similar modification is made for cell (i−1, j) when its partner cell (i−1, j−1) is being dealt with. Similarly in cell (i,j−1) the pressure force on the west side is magnified by the factor above. fluxes from the interface computed in cell (i, j−1) are assigned to cell (i,j) and from cell (i−1,j−1) to cell (i−1,j). Thus, the partner assignment procedure and the cut cell coefficient assembly algorithms achieve explicit flux conservation in the cells affected by the interface.

2.10 Anomalous cases

However, some anomalous situations may be encountered in the coefficient assembly process. For instance, in Figure 10 , the u−control point (i,j) is adjoined by a solid phase control point. Therefore the flux through the east face is not straightforward to compute. The way this is done to maintain consistency at that face is by noting that cell (i+1,j+1) has been redefined by the partner cell assignment procedure to be of the shape shown. Thus, a part of the west face of cell (i+1,j+1) is now adjacent to the east face of cell (i,j). Therefore, the flux through the west face of cell (i+1,j+1) has to be consistent with the fluxes

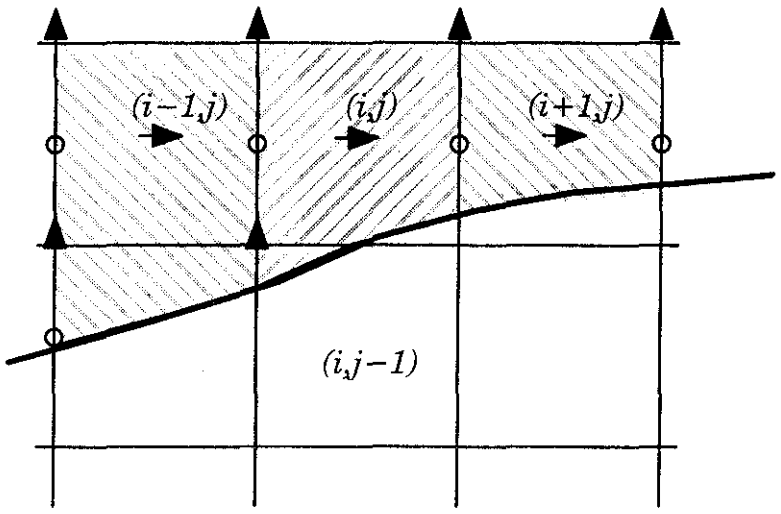

Figure 9
Illustration of partner cell definitions

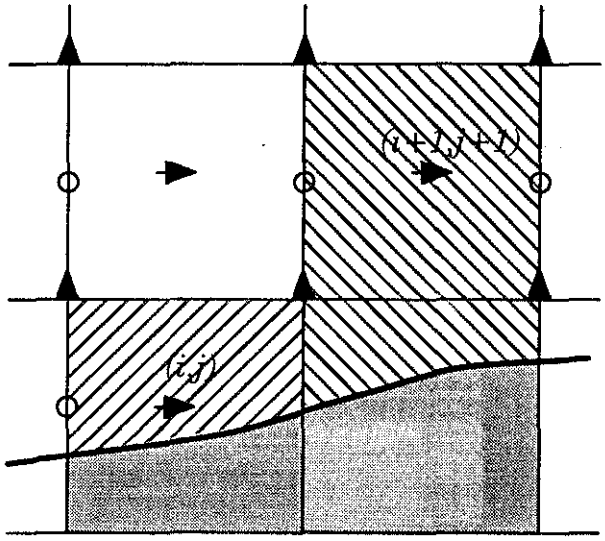

Figure 10
Illustration of an anomalous case in defining fluxes

through the east faces of (i,j) and (i,j+1). The flux through the east face of cell (i,j) is now obtained by redistributing the west face flux of cell (i+1,j+1), weighted according to the dimensions $dl_e(i,j)$ and $dl_e(i,j+1)$. In addition, if the east face pressure control point of cell (i,j) is also in the solid phase, the pressure contribution from cell (i+1,j+1) is redistributed consistently between cells (i,j+1) and (i,j). Such anomalous cases exist for all eight types of cells and for all control volumes. Treating such cases adds to the tedium of assembly of the coefficients but is critical in obtaining solutions to flow problems. If consistency at cell faces is violated, convergence cannot be achieved due to the existence of the spurious sources/sinks of mass, momentum and energy at such locations.

2.11 Distinction between liquid and solid cells

In the cell assembly procedure, one has to be careful not to step across the interface into the opposite phase in performing the flux computations. The advantage in combining the Eulerian (field solver) and Lagrangian (interface tracking) methods here is that the two phases can be treated separately. Thus, unlike in the Eulerian methods, the interface separating the two phases can be explicitly defined and treated as a discontinuity. And, in contrast with the Lagrangian methods, grid redistribution for conformity with the moving, distorting boundary is avoided. Thus, in each phase, the operations involved in obtaining the flux estimates should involve points in the same phase , and the interfacial values only. The treatment of the liquid and solid phase control points follows the same procedure as far as the coefficient assembly is concerned. However, the solid is passive as far as fluid flow is concerned, unlike in the purely Eulerian methods, where it is assumed to have some porosity in the proximity of the interface to ease the sudden property jump across it. In our case, once the coefficients are assembled, a flag denoting solid is employed to turn off the fluid flow computations in the solid phase, such that $a_P = 1$ and a_E, a_W, a_N, a_S , $b=0$ in the solid., which results in $u=v=p' =0$ in the solid phase. This, of course is not applicable for the energy equation where heat conduction in the solid is to be accounted for.

2.12 Moving boundary problems – treatment of cells that change phase

When the interface moves, say due to change of phase, the shape of the interface at two time instants (or iterations) may develop as shown in Figure 11.

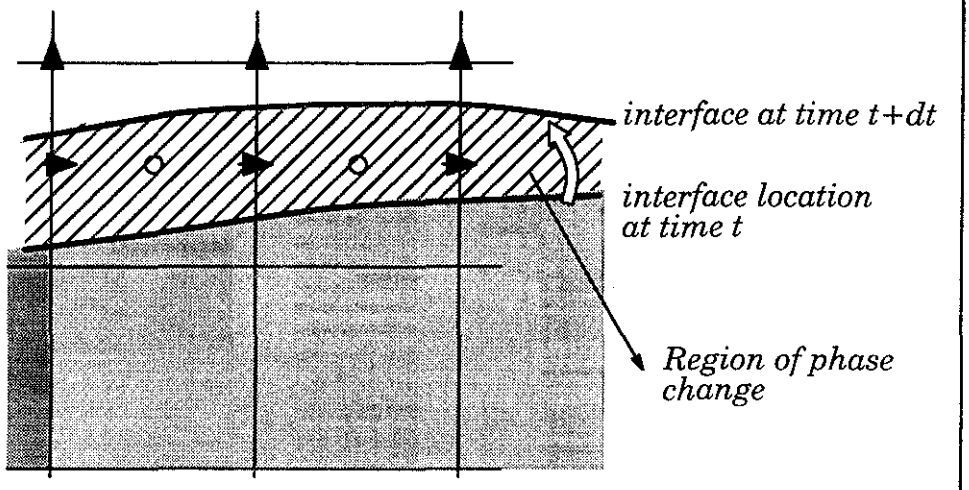

Figure 11
Change of phase of cells as the interface traverses the domain

Thus cells (i,j), (i+1,j) etc. have moved from solid phase into the liquid. In the implicit solution procedure adopted here, information regarding the previous state of a control point is required to evaluate the time derivative, i.e., the quantity $\phi^n_{i,j}$ corresponding to the new phase is non–existent for that control point. To overcome this difficulty, flags are employed indicating the current and previous phases of the control point. When a control point changes phase, the value at that location corresponding to the phase in which it finds itself is estimated by performing a linear interpolation as shown in Figure 12. The new value in a cell which undergoes phase change is thus obtained by interpolation from neighbouring cells in the same phase as

$$\phi^n_{ij} = (dy_I \phi^n_{ij+1} + dy_N \phi^n_I)/(dy_I + dy_N) \qquad (48)$$

In particular the value $\phi^n_{i,j}$ is then obtained via the implicit solution procedure by iteration. In our computations, flipping of a control point between two phases was practically non–existent. This problem exists in purely Eulerian methods. In our case, since the interface is a continuous entity each point on the

interface is influenced by the motion of all its neighbours along the interfacial curve and this global influence helps in avoiding flipping of phase. The interface reconstruction procedures rely on local fluid fraction information in a cell, to define the interface and thus it is possible for a cell to flip between phases in the course of the iterations.

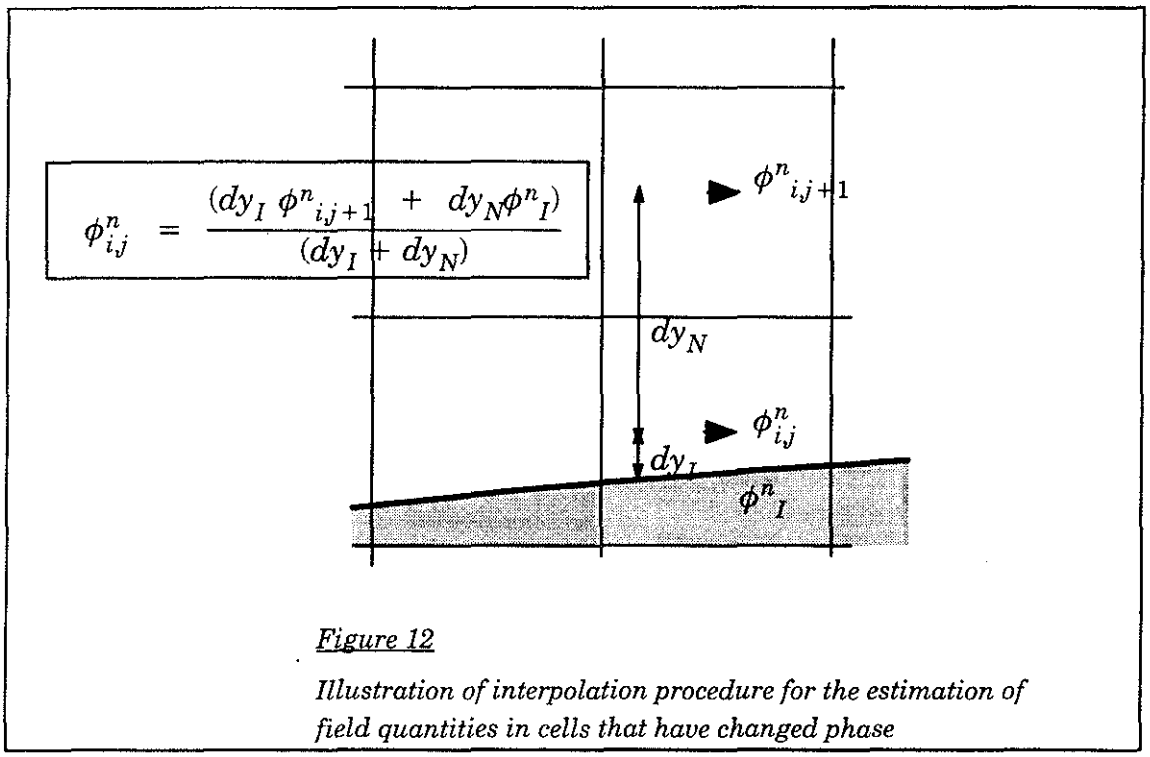

Figure 12

Illustration of interpolation procedure for the estimation of field quantities in cells that have changed phase

3. Results and discussion

We first compare solutions for a stationary interface with those from well–tested solution procedures using body–fitted coordinates [25]. This exercise is designed to validate the conservation and consistency characteristics of the cut cell method. The interface is sufficiently deformed that all the types of cut cells are encountered. In the absence of a consistent discretization in the vicinity of the interface, it is found that convergence cannot be achieved, and that care needs to be exercised in performing flux calculations in the grid cells affected by the interface. The computational domain is as shown in Figure 13(a). The square cavity is a frequently adopted test bed for numerical experiments for incompressible flows and benchmarks exist. We deform the base of the cavity , the amplitude being 10 per cent of the base. A 121x121 cartesian grid is employed. We first present the results for a driven cavity flow, where the top wall of the cavity is pulled at velocity U = 1 corresponding to a Reynolds number of 1000. The results from the present method is compared with a previously benchmarked body–fitted formulation with the same grid size. The results are shown in Figure 14. The streamline patterns in Figures 14(a) and (b) show good agreement. A quantitative comparison can be seen in Figures 14(c) and (d) where the centerline velocities are plotted.

In Figure 15 we compare the results for a stationary interface with natural convection in the cavity shown in Figure 13 (b). The same grid size and interface shape as above is used. The Rayleigh number computed is 10^5 and Pr =1. Again the streamline patterns shown in Figures 15 (a) and (b) are in good agreement. In Figure 15(e), (f), (g) we compare the centerline values of u, v components of velocity and temperature respectively along the centerline of the cavity. The results agree closely with the body–fitted code. Thus, it has been shown that the current scheme yields accurate results for the case of a stationary interface, in the presence of complex flowfields. It is noted here that the formulation developed here would be useful

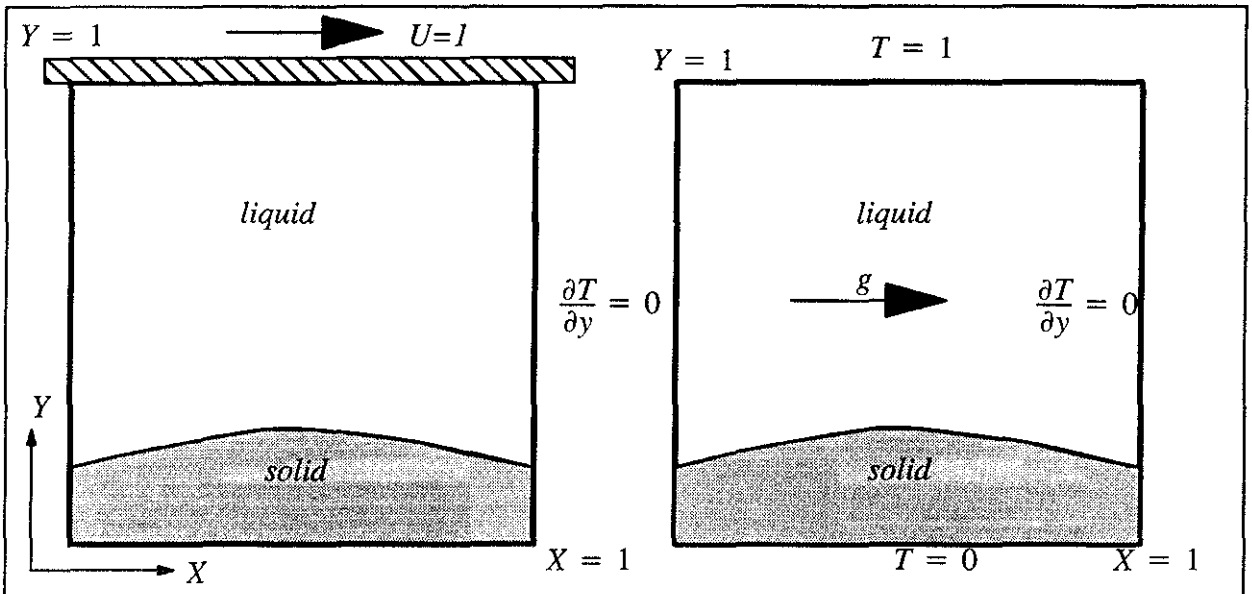

(a) Driven cavity flow *(b) Natural convection*

Figure 13

Illustration of computational domain and boundary conditions for the test cases presented. For both configurations, no–slip conditions are applied on all solid surfaces. A cartesian grid is used, with the interface passing through the grid. The interface amplitude was equal to 0.1, which is 10% of domain size.

in computing incompressible flows around complex shapes employing fixed Cartesian grids, circumventing the need for generation of boundary–fitted grids.

We now proceed to test the numerical procedure developed here for a situation involving phase change. Hitherto much effort has been devoted to numerically duplicating the results of Gau and Viskanta [26] (hereafter referred to as G&V) for the melting of Gallium from a vertical wall in a rectangular enclosure. Gallium is adopted as the experimental material since it is a metal with low melting point and thus is easy to handle. Unfortunately numerical values of interface positions were not presented in G&V and the initial conditions are ambiguous. The authors also present interface shapes viewed form the front and rear of their experimental set–up, and poor correspondence is observed. Furthermore, recent experiments of Campbell et al. [27] appear to differ from G&V in regard to interface shapes and positions. Underlying these facts is the difficulty in performing experiments in relation to flowfields and interface positions in opaque melts. Despite these limitations, the experiments of G&V have been extensively employed for comparison. Needless to say, the agreement between the numerics and experiment is at best modest [28]. A more effective comparison may be between numerical techniques of essentially disparate nature, for instance purely Lagrangian and Eulerian methods. Lacroix and Voller [29] have performed such a comparison. The grid sizes used by these authors, however may not be sufficiently fine to resolve all the flow features. In our work, we found the presence of multiple convection cells in the initial stages of development of the interface in some cases. It is not conceivable that such cells can be resolved by coarse grids. The presence of such cells is important to capture, in particular because the interface shape reflects the presence of these flow features. Thus, two different numerical schemes can yield the same results for the same grid spacing, but neither may actually be an accurate calculation. In fact, the level of numerical dissipation, i.e., the order of accuracy of the numerical technique was found to determine the types of flow features resolvable, especially at higher Rayleigh numbers. Thus, the entire situation, especially for the higher Rayleigh numbers, is found to be highly sensitive to the numerical conditions employed. Since

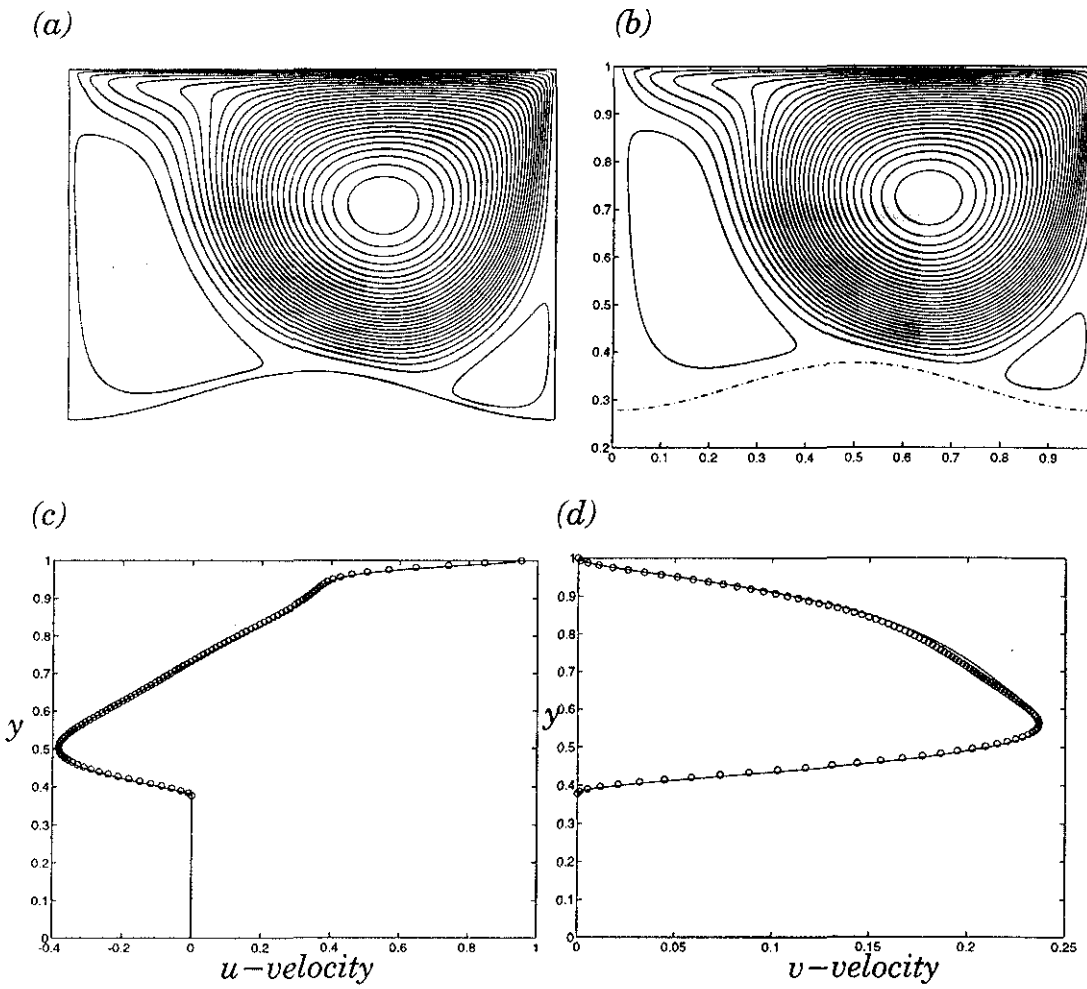

Figure 14

Streamlines for the case of a driven cavity with a deformed base. Re=1000, 121x121 grid. (a) Contours from a boundary−fitted grid computation. (b) On a fixed Cartesian grid using the current method.

Comparison of solutions from the boundary−fitted and current Cartesian grid method. (c) Centerline u−velocity. Dots represent solution from boundary−fitted grid. Full lines from current calculation. (d) centerline v−velocity.

the interface shape is strongly linked to the flow features and vice−versa, great care must be employed in performing the computations.

Here we present calculations for the melting of Gallium from a vertical wall for the configuration shown in Figure 16. The current method is compared with an enthalpy−based Eulerian method [30] employing an 81x81 grid. Unless otherwise mentioned the second−order central difference scheme is used for both the methods. In a method dealing with the temperature as a variable and using an interface tracking procedure, it is not possible to initiate melting in a domain that is entirely solid. Thus, the computations using the present method is started from an initial condition generated by the enthalpy method, so that an thin initial melt layer exists at the start. The flowfield and temperature field are obtained form the purely Eulerian method. Melting is initiated at the left wall. In Figure 17 we show the results for a Rayleigh number of 10^4. The Prandtl number of Gallium is 0.021. The Stefan number for this case is 0.042. The interfacial shape and position are compared in this case with that of the enthalpy−based method in Figure 17(a). As can be seen close agreement is maintained between the predictions of the two methods. The present interface tracking method is marginally slower than the purely Eulerian method for large times. However, it

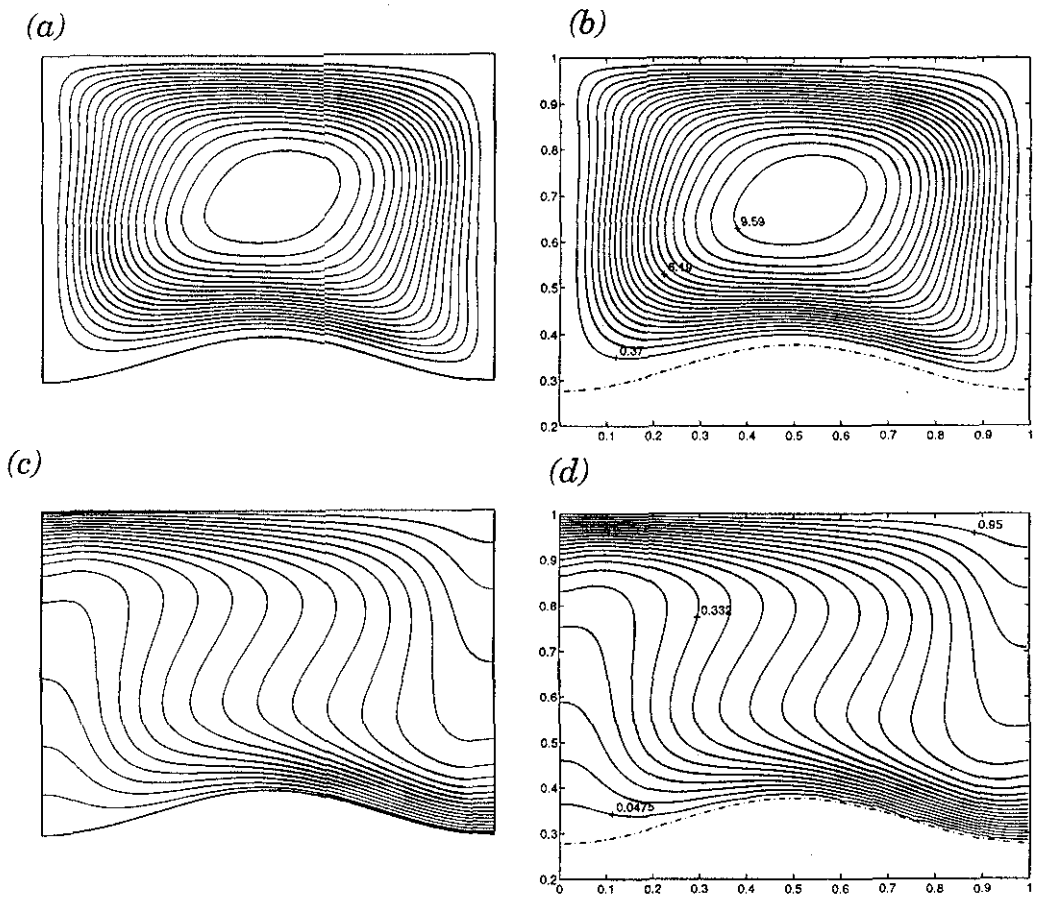

Figure 15

Streamlines for natural convection in a deformed cavity. Re=10^5, Pr=1, 121x121 grid. (a) Result from boundary–fitted grid computations. (b) Results from Cartesian grid computations.
(c) Isotherm contours from the boundary–fitted formulation. (d) Isotherm contours from the Cartesian grid computations.

is likely that with further refinement of the grid better agreement can be obtained. It may be noted that the location of the elbow in the phase front is correctly predicted, and thus the size of the recirculation zone is obtained accurately. This can be seen from the plots of the streamlines at two different time instants, shown in Figure 17 (c–f). Furthermore the centerline velocities and temperature profiles, shown in Figure 17 (b) are in good agreement. Thus this experiment has proven that the methods employed in treating the interface, in particular the flux computations for the cut cells, the treatment of pressure terms, and the procedures involved with the newly formed cells are borne out by these calculations.

We next present, in Figure 18 the results for a higher Stefan number. In this case, as above Ra= 10^4, Pr=0.021, but Stefan number St=0.42, a ten–fold increase. In Figure 18(a) the interface positions are compared, plotted at equal intervals of time $\delta t^* = 10$. As can be seen the results are very close except for the lagging of the current method for larger times. But even for the rapidly moving interface, the front shapes are well predicted, which implies that the bulk flow, i.e., recirculation zones are obtained accurately. In the figures containing contours of streamfunction and isotherm contours, Figures 18 (c–h), the interface has been represented in each case by plotting the temperature contours T=–0.005, 0.0 and 0.005. In the case of the enthalpy method this is the best approximation to the interface shape that one can ob-

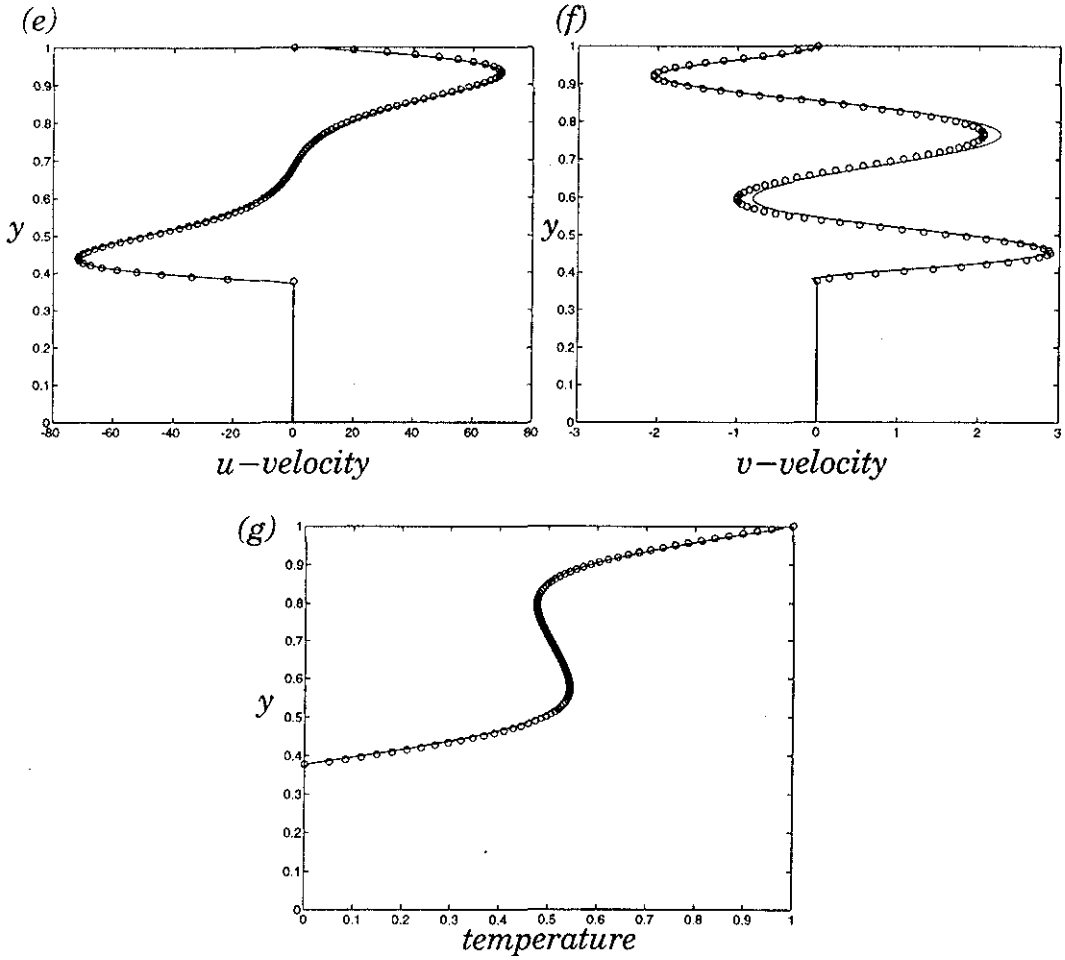

Figure 15 (contd.)

(e) Centerline u−velocity. Dots are from the boundary−fitted grid computations. Full lines are from the current method. (f) Centerline v−velocity comparison. (g) Centerline temperatures.

tain. In fact, in the comparisons of the interface shapes, the values corresponding to the enthalpy method are obtained as that corresponding to the $f_s = 0.5$ contour by interpolation. Thus there is an uncertainty of the order of the grid spacing in identifying the interface position in the enthalpy method. In contrast the interface tracking procedure explicitly yields information regarding interface shape. Also, it is noted that in the interface tracking method, no modelling of physics is necessary in the vicinity of the interface, while in the enthalpy method, there is an unavoidable smearing of information. In addition the D'Arcy law treatment and the mushy zone model [31] obscure the transport processes in this region.

The results presented above were applicable to phase change at the macroscopic scale. The interface at such scales is only mildly distorted as seen in Figures 17 (a) and 18(a). However at the microscopic levels, the interface can be highly deformed and can assume highly branched forms called dendrites and deep cellular morphologies. The transport mechanisms at that level are dominated by thermal diffusion. However, significant effects of convection have been reported [32,33,34]. We present in Figure 19 below results of computations performed at the microscopic level in the absence of convection [11]. The results for such diffusion−controlled growth demonstrate the expected effects of surface tension at the microscopic level. For low interfacial tension (Figure 19(a)), the interface is sensitive to perturbation and tends to break down into branched structures. The noise level and resolution of the front features during the breakdown of the interface are strongly dependent on the grid resolution available. For sufficient interface tension

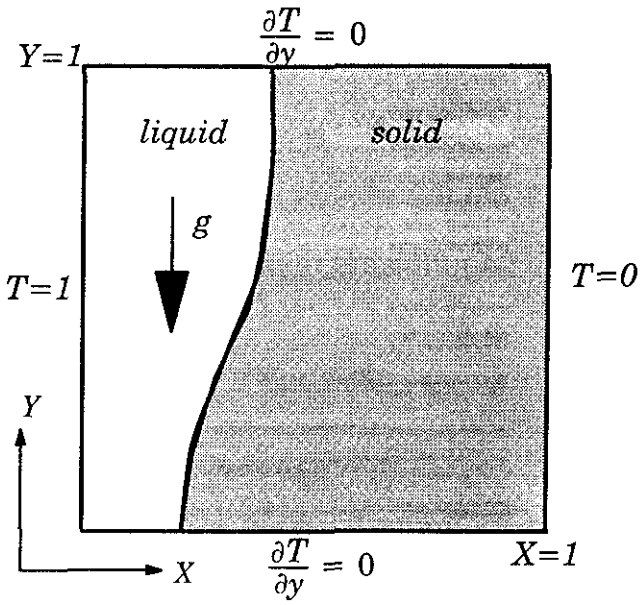

Figure 16

Illustration of computational domain and boundary conditions for the melting of Gallium. The melting is initiated at the left wall. No−slip velocity conditions are imposed on all solid surfaces. Computations are performed on a cartesian grid.

however, the results have been demonstrated to converge under grid refinement. The initial perturbation develops in time into long fingers (Figure 19(b)), as in the analogous Saffman−Taylor instability. The method is thus shown to be capable of tracking evolving interfaces for large times and distortions. Computations of microstructure evolution with effects of convection included are in progress.

4. Summary

The *ELAFINT* has been developed to combine the strengths of the purely Eulerian and Lagragian methods. This has resulted in a method that has the following features.

1. Highly distorted interfaces can be handled by the Lagrangian component, namely the interface tracking scheme. In previous work [22] we have demonstrated the ability of the scheme to capture the interactions, i.e. merger and breakup of different shapes and their subsequent evolution. The methods that were developed to handle diffusion−controlled instability phenomena [11] have here been extended to incorporate convection effects.
2. The computations are performed on a fixed Cartesian grid. Thus, the problems associated with grid redistribution associated with body−fitted adaptive grids is avoided. Also the procedures employed in the discretization of the equations on such a grid lend themselves to the use of well −tested implicit pressure−based flow solvers. The solutions are achieved by discretizing the equations via a control volume formulation, with particular attention toward conservation and consistency in assembling the fluxes of conserved variables. The solution is achieved by using the line SOR method, leading to the iterative solution of tri−diagonal matrices.
3. The interface definition is strictly maintained and the boundary conditions applied on the control volumes. The release of latent heat during phase change has been incorporated via the Stefan condition. Several details involved in dealing with the presence of the interface have been presented. Some procedures have been devised in dealing with the flux of quantities at the interface.

The results presented here demonstrate the accuracy of the computational procedure by comparing with previously tested methods. Further extension of the work here to incorporate the effects of convection at the microstructural level is now underway.

Acknowledgements :
The work presented here was partially supported by the AFOSR/URI Program and GE Aircraft Engines. Computations were performed on the CRAY−YMP at Eglin Air Force Base, Pensacola, Florida.

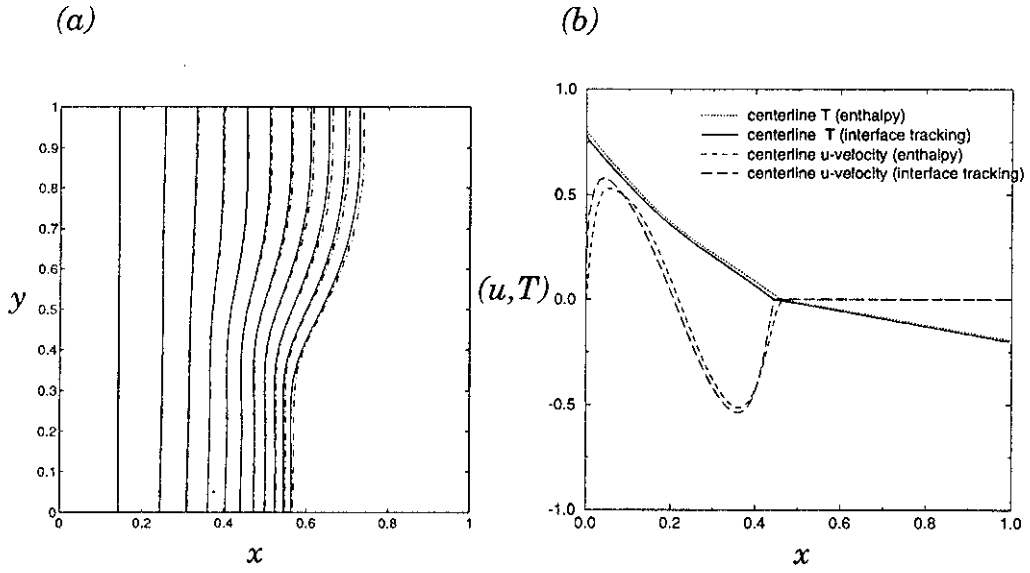

Figure 17

Melting of Gallium, $Ra=10^4$, $Pr=0.021$, $St=0.042$, 81x81 grid. Melting is initiated at the left. (a) Comparison of interface positions at equal intervals of time. Dotted lines represent the enthalpy−based method, full lines correspond to the present method. (b) Comparison of centerline profiles.

5. References

1. Crank, J. (1984) , *Free and Moving Boundary Problems,* Oxford University Press, Oxford, UK.
2. Floryan, J. M. and Rasmussen, H. (1989) , " Numerical methods for viscous flows with moving boundaries," *Appl. Mech. Rev.,* Vol. 42, No. 12, pp. 323−341.
3. Thompson, J.F., Warsi, Z. U. A., and Mastin, C.W. (1985), *Numerical Grid Generation,* Elesevier , New York.
4. Shyy, W., Udaykumar, H. S. and Liang, S.−J. (1993) , " An interface tracking method applied to morphological evolution during phase change," *Int. J. Heat Mass Transf.*, Vol. 36, No. 7, pp. 1833−1834.
5. Shyy, W., " An adaptive grid method for Navier−Stokes flow computation," *Appl. Math. Comput.* , Vol. 21, pp. 201−219, 1987.
6. Hirt, C. W. and Nichols, B. D. (1981) , " Volume of Fluid (VOF) method for the dynamics of free boundaries," *J. Comp. Phys,* Vol. 39, pp. 201−225.
7. Sethian, J. A. (1990), " Numerical algorithms for propagating interfaces : Hamilton−Jacobi equations and conservation laws," *J. Diff. Geom.,* Vol. 31, pp. 131−161.

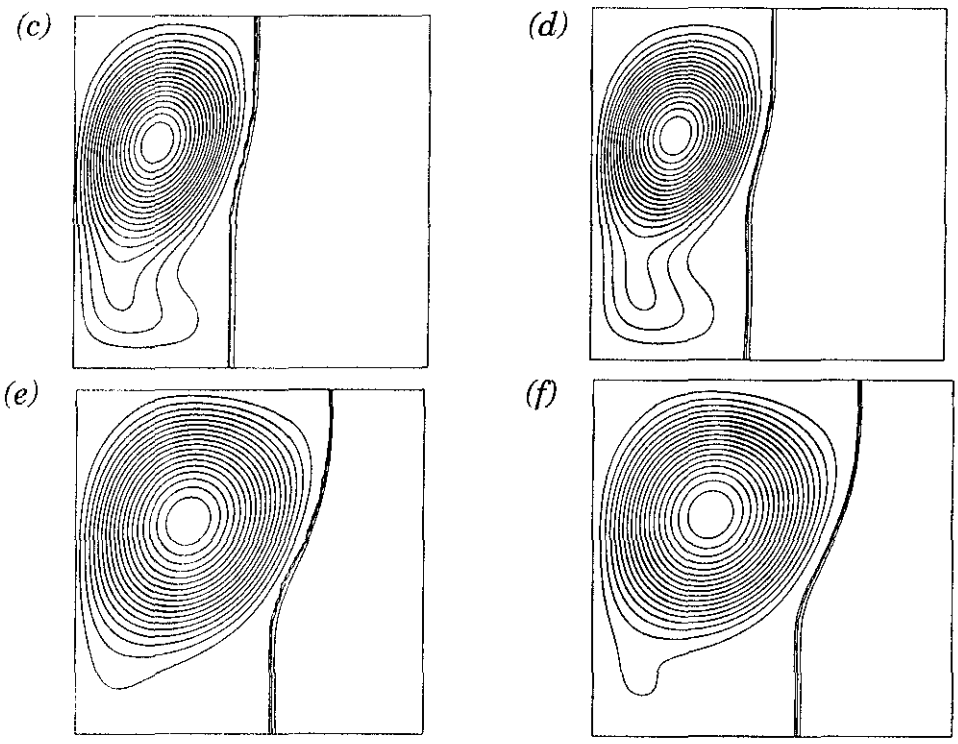

Figure 17 (contd.)

Streamline contours at t=50 and t=100. Comparison of the enthalpy and present methods. (c) Current interface tracking method, t=50. (d) Enthalpy method, t=50. (e) Current method, t=100. (f) Enthalpy method, t=100. The interface has been represented by plotting the temperature contours between T=−0.005 and 0.005. In the case of the current method, the interface position is actually available explicitly and exactly. In the enthalpy method, the only information regarding the interface is the contours shown.

8. Kobayashi, R. (1993), " Modelling and numerical simulations of dendritic crystal growth," *Physica D.*, Vol. 63, pp. 410−423.
9. Wheeler, A. A., Murray. B. T., and Schaefer, R. J. (1993) , " Computations of dendrites using a phase field model, " *Physica D.*, Vol. 66, pp. 243−262.
10. Liang, P. Y., (1991) "Numerical method for calculation of surface tension flows in arbitrary grids," *AIAA J.* , Vol. 29, No. 2, pp. 161−167.
11. Udaykumar H. S. and Shyy, W. (1994), "Simulation of interfacial instabilities during solidification; part I : conduction and capillarity effects," to be published.
12. Miyata, H. (1986), " Finite difference simulation of breaking waves," *J. Comp. Phys.*, Vol. 65, pp. 179−214.
13. Morinishi, K. (1992), " A finite difference solution of the Euler equations on body−fitted Cartesian grids," *Comput. Fluids,* Vol. 21, No. 3, pp. 331−344.
14. Quirk, J. J. (1992) , " An alternative to unstructured grids for computing gas dynamic flows around arbitrarily complex two−dimensional bodies," *ICASE Report No. 92−7,* NASA Langley Research Center, Hampton, VA.
15. Zeeuw, D. D. and Powell, K. G. (1990) , " An adaptively−refined cartesian mesh solver for the Euler equations," AIAA Paper 90−0000.
16. Bayyuk, S. A., Powell, K. G. and van Leer, B. (1993), " A simulation technique for 2−D unsteady inviscid flows around arbitrarily moving and deforming bodies of arbitrary geometry," AIAA Paper No. 93−3391.
17. Kothe, D. B. and Mjolsness, R. C. (1992) , " RIPPLE : A new method for incompressible flows with free surfaces," *AIAA J.*, Vol. 30, No. 11, pp. 2694−2700.

18. Kessler, D.A., Koplik, J. and Levine, H. (1988) ,"Pattern selection in fingered growth phenomena," *Advances in Physics*, Vol. 37, No. 3, pp. 255–339.
19. Langer, J.S. (1980) , " Instabilities and pattern formation in crystal growth," *Rev. Mod. Phys.*, Vol. 52, No.1, pp. 1–56, 1980.
20. Glicksmann, M.E., Coriell, S. R. and McFadden, G. B., "Interaction of flows with the crystal–melt interface," *Ann. Rev. Fluid Mech.*, Vol. 18, pp. 307–336, 1986.
21. Ostrach, S. (1983), " Fluid Mechanics in Crystal Growth," *J. Fluids Engg.*, Vol. 105, pp. 5–20.
22. Udaykumar, H.S. and Shyy, W. (1993) , " Development of a grid–supported marker particle scheme for interface tracking," *11th AIAA Comp. Fluid. Dyn. Conf., Paper No. AIAA–93–3384,* Orlando, Florida.
23. Wang, J.C.T. and Widhopf, G.F. (1989), " A high–resolution TVD finite volume scheme for the Euler equations in conservation form," *J. Comp. Phys.*, Vol. 84, pp. 145–173.
24. Patankar, S.V. (1980), *Numerical Heat Transfer and Fluid Flow,* Hemisphere Publishing Corp., Washington D.C..
25. Shyy, W. (1994), *Computational Modelling for Fluid Flow and Interfacial Transport*, Elsevier, Amsterdam, The Netherlands.
26. Gau, G. and Viskanta, R. (1986), " Melting and solidification of a pure metal on a vertical wall," *Trans. ASME*, Vol. 108, pp. 174–181.
27. Campbell, T. A., Pool, R. E. and Koster, J. N. (1994), " Melting and solidification of a liquid metal at a vertical wall," AIAA Paper No. 94–0792.
28. Lacroix, M., "Computation of heat transfer during melting of a pure substance from an isothermal wall, " Numer. Heat Transfer, Part B, Vol. 15, pp. 191–210, 1989.
29. Lacroix, M. and Voller, V. R. (1990), " Finite difference solutions of solidification phase change problems: transformed versus fixed grids," *Numer. Heat Transf. Part B*, Vol. 17, pp. 25–41.
30. Shyy, W. and Rao, M. M. (1993), " Enthalpy based formulations for phase change problems with application to g–jitter," AIAA Paper No. 93–2831, also *Microgravity Sci. and Tech.*, Vol. 7 (1994), pp. 41–49.
31. Voller, V. R. and Prakash, C., "A fixed grid numerical modelling methodology for convection–diffusion mushy region phase change problem," *Int. J. Heat and Mass Transfer,* Vol. 30, pp. 1709–1719.
32. Bouissou, Ph., Perrin, B. and Tabeling, P. (1990) , "Influence of an external periodic flow on dendritic crystal growth," in *Nonlinear Evolution of Spatio–temporal Structures in Dissipative Dynamical Systems,* Eds. F. H. Busse and L. Kramer, Plenum Press, New York.
33. Sato, T., Kurz, W. and Ikawa, K. (1987) , " Experiments on dendrite branch detachment in the Succinonitrile–Camphor alloy," *Trans. Japan Inst. Met.*, Vol. 28, No. 12, pp. 1012–1021.
34. Tirmizi, S. H. and Gill, W.N., "Effect of natural convection on growth velocity and morphology of dendritic ice crystals," J. Crystal Growth, Vol. 85, pp. 488–502, 1987.

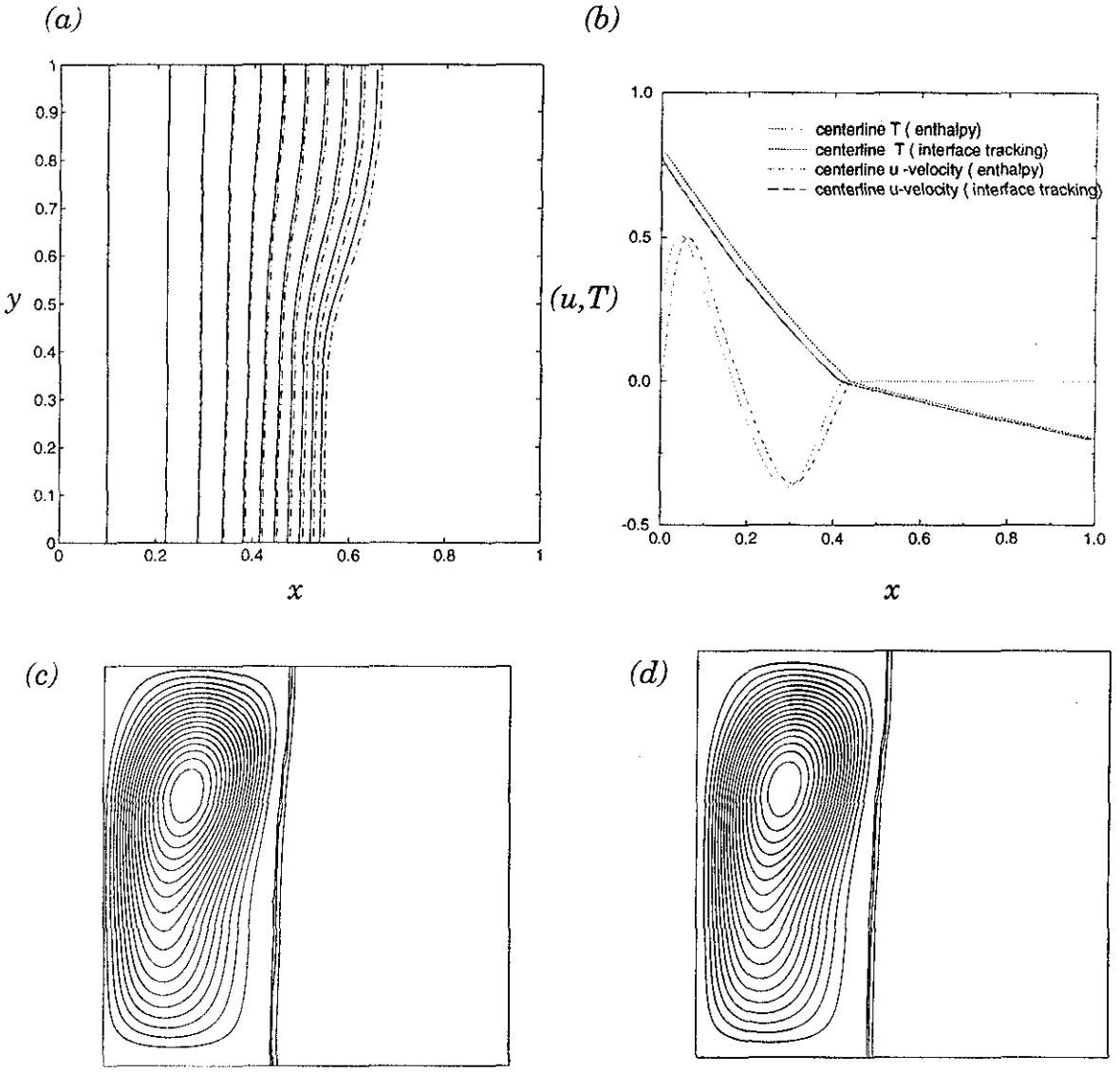

Figure 18

Melting of Gallium. Comparison of solutions from an enthalpy method and the present interface tracking method. Higher Stefan number case. $Re=10^4$, $Pr=0.021$, $St=0.42$, 81x81 grid. (a) Comparison of interface shapes at equal intervals of time. Full lines belong to the present method. Dashes represent enthalpy method. (b) Comparison of centerline values. The legend is self−explanatory. (c) Streamline contours for the current method at $t=50$. (d) Streamline contours for enthalpy method at $t=100$. In (c) and (d), the interface is represented by plotting the temperature contours $T=-0.005$, 0.0 and 0.005.

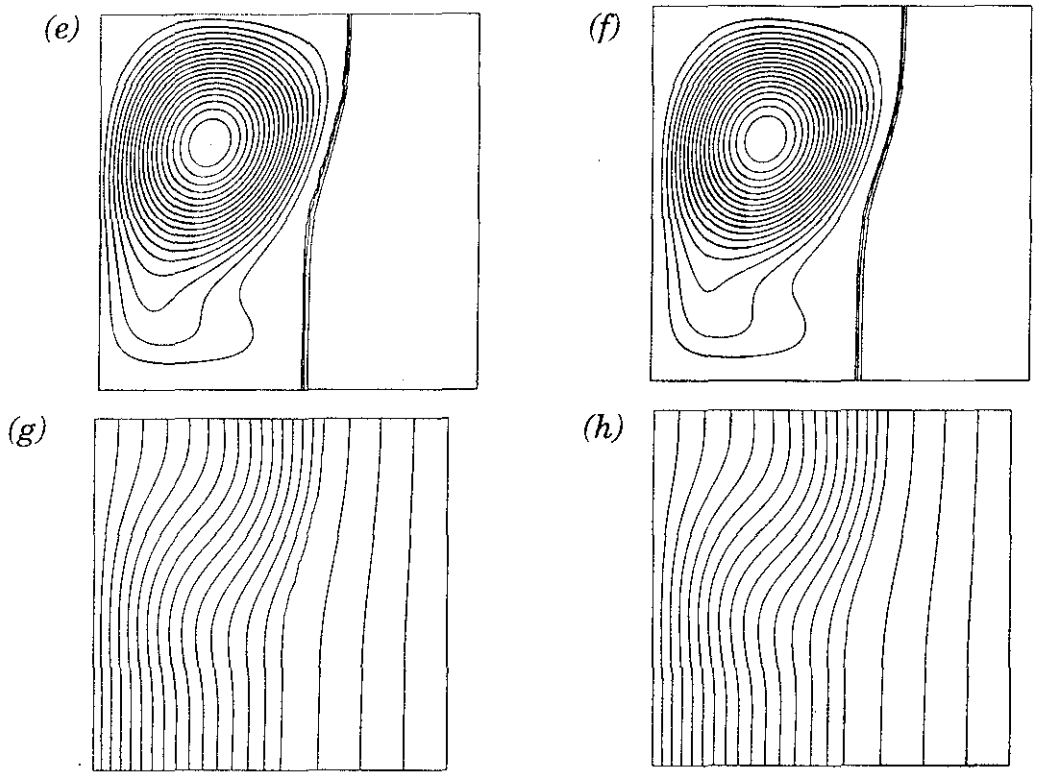

Figure 18 (contd.)

(e) Streamline contour at t=100, for the interface tracking method. (f) Streamline contour at t=100, enthalpy method. (g) Isotherms at t=100, interface tracking method. (h) isotherms at t=100, enthalpy method.

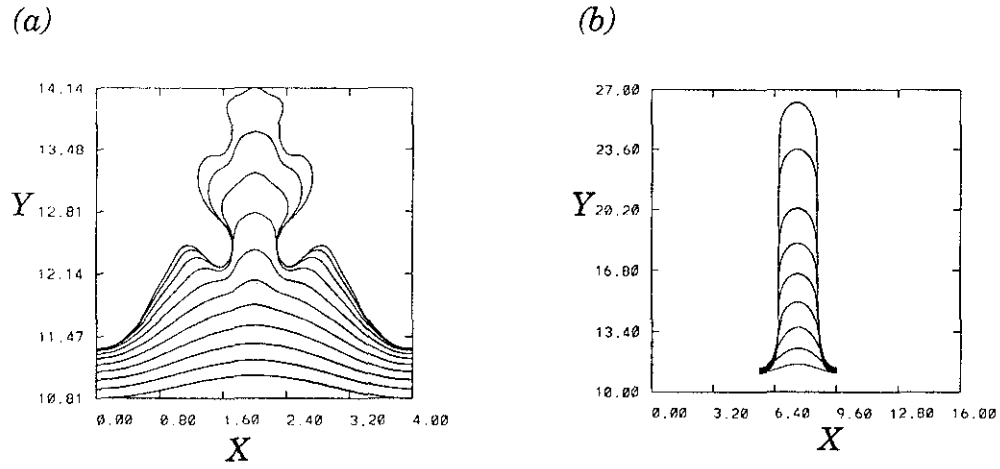

Figure 19

(a) Interface shapes for low surface tension. Successive instabilities lead to branched structure. Each line corresponds to the interface shape at a given instants.
(b) Interface evolution for higher surface tension. A stably propagating finger is obtained.